ANALYSIS FOR CONFINEMENT LOSS IN ADVANCE V-SHAPED PCF BASED Au-SPR BIOSENSOR

By

NIVEDITA KAR * ANKITA KAR **

MAYANK SINGH *** DEEPAK YADAV ****

*-** Assistant Professor, IERT, Prayagraj.
-* Student, Department of Electronics Engineering, IERT, Prayagraj.

Date Received: 26/05/2025 Date Revised: 04/06/2025 Date Accepted: 13/06/2025

ABSTRACT

This paper introduces an advanced V-shaped photonic crystal fiber (PCF)-based surface plasmon resonance (SPR) biosensor. Numerical analysis of the sensor is carried out using the finite element method (FEM) in COMSOL Multiphysics 6.2. This incorporation of a V-shaped geometry improves the coupling between the core-guided mode and the surface plasmon mode, leading to optimized wavelength sensitivity and minimized confinement loss. The proposed sensor design is capable of detecting the analytes within a refractive index range of 1.38 to 1.42, making it suitable for applications in biochemical and biological detection, including drug analysis, antigen-antibody interactions, and gas sensing.

Keywords: Confinement Loss, Photonic Crystal Fiber (PCF), Surface Plasmon Polaritons (SPP) and Surface Plasmon Resonance (SPR).

INTRODUCTION

Surface Plasmon Resonance (SPR) is a well-known phenomenon in numerous photonic sensors, including prism-based SPR sensors, PCF-based sensors, and traditional optical waveguide-based sensors. This optical resonance effect occurs when free electrons vibrate at the interfacing boundary of metal and dielectric in sensors. Surface plasmon polaritons (SPP), or plasmonic waves on the sensor surface, are produced by the vibration of these free electrons, which travel all along the metallic material's boundary (Zhan et al., 2018). The SPR phenomenon is well known for its ease of use and sensitivity in determining the refractive index (RI) of a variety of materials in their liquid, solid, and gaseous phases (Gupta & Sharma, 2005; Otto, 1968; Peng et al., 2015; Piliarik et al., 2003; Verma et al., 2011). Recently, surface plasmon resonance (SPR) sensors have attracted researcher's attention for their real-time, label-free detection capabilities, especially in biochemical and environmental applications. The SPR phenomenon arises due to resonant oscillation of conduction electrons at the interface between a metal and dielectric, which is highly sensitive to changes in the refractive index (RI) of the surrounding medium (Homola, 2008). This makes SPR an ideal mechanism for detecting minute RI variations, relevant in biosensing and chemical sensing (Willets & Van Duyne, 2007).

In earlier developments, prism-coupled configurations like the Kretschmann and Raether (1968) setups were extensively used for excitation of surface plasmons in planar structures. While these systems offered valuable insights and sensitivity, they lacked compactness and integration potential. To overcome these limitations, traditional prism-based SPR setups evolved into more

i-manager Publications
Member of:
This paper has objectives related to SDG
9 INDUSTRY, INNOVATION AND INFRASTRUCTURE

compact and integrated platforms using optical fibers. Among these, photonic crystal fibers (PCFs) offer a versatile and powerful platform due to their micro-structured cladding that allows unique control over modal properties and light confinement (Russell, 2003). PCFs have been integrated with SPR mechanisms to enhance sensor miniaturization and improve sensitivity (Hassani & Skorobogatiy, 2006). Fiber-optic SPR biosensors, such as D-shaped, U-shaped, and tapered fiber sensors, offered miniaturization, flexibility, and remote sensing advantages (Gupta & Verma, 2009; Zhang et al., 2017). The evolution continued with the introduction of more sophisticated geometries like H-shaped and V-shaped PCFs. V-shaped designs gained interest because of their superior confinement of light near the metal interface, which improves the overlap between the core mode and plasmonic mode, enhancing the sensor's responsiveness (Abdelghaffar et al., 2023).

The V-groove structure ensures efficient coupling of light to the plasmonic surface, increasing the sensor's overall sensitivity and reducing propagation loss (Huraiya et al., 2024). Gold and silver remain the most commonly used plasmonic materials. Silver is often used in SPR sensors due to its sharp resonance and low damping, which result in a highly sensitive and clear signal. Damping refers to the loss of energy as the surface plasmons oscillate, and low damping means these oscillations persist for longer without significant energy loss. This leads to a sharper resonance peak, enhancing the sensor's sensitivity. However, silver is prone to oxidation when exposed to air and moisture, forming a layer of silver oxide that negatively impacts its performance. To prevent this, titanium dioxide (TiO_2) is commonly used as a protective layer. TiO_2 provides excellent chemical stability and forms a barrier between silver and the surrounding environment, protecting the silver from oxidation without interfering with its plasmonic properties; however, such damage results in a complex fabrication procedure. Thus, to make fabrication a simple process, gold has been favored as a plasmonic material due to its excellent biocompatibility and chemical stability (Sharma et al., 2007).

The performance of an SPR sensor is judged based on key metrics such as confinement loss, wavelength sensitivity, resolution, and figure of merit (FOM). Wavelength sensitivity in biosensors refers to the shift in the resonant wavelength due to a change in the surrounding refractive index. A highly sensitive biosensor shows a larger wavelength shift for a small variation in the analyte's refractive index, allowing better detection of minor surrounding changes (Sharma et al., 2007). Similarly, the term 'figure of merit' evaluates the efficiency of a sensor by considering both its sensitivity and the sharpness of the resonance curve. FOM combines sensitivity and sharpness of the resonance dip to give a single value representing overall sensor performance. A higher figure of merit implies that the sensor not only responds strongly to refractive index changes but also maintains a narrow and distinct resonance (Gupta & Sharma, 2005). A biosensor with high resolution is capable of identifying very minor variations, which is essential for precise and early-stage detection applications. This parameter of the sensor, i.e., resolution, defines the smallest change in the analyte's refractive index that the sensor can accurately detect (Homola, 2008). The last parameter of the SPR sensor is confinement loss, which indicates how much optical energy leaks out of the guiding structure into the surrounding medium. In SPR biosensors, a higher confinement loss at the resonance point reflects stronger interaction between the optical field and the plasmonic surface, resulting in a noticeable dip in the output spectrum (Abdelghaffar et al., 2023). Optimizing these parameters requires careful control over the fiber structure, metal layer thickness, and analyte region configuration (Sardar & Faisal, 2024).

In this paper, an advanced V-shaped PCF-based SPR sensor is modeled and simulated using COMSOL Multiphysics 6.2, which provides a finite element method (FEM)-based approach for analyzing optical mode propagation and loss characteristics (COMSOL, 2023). The simulation involves eigenmode analysis to determine the effective index, confinement loss, and sensitivity across various design configurations (Mim et al., 2025). Parametric sweeps and performance analysis were

carried out to examine how variations in core geometry, thickness of the plasmonic metal coating, and changes in the analyte's refractive index influence the sensor's optical response. The objective is to analyze and minimize confinement loss across different design configurations, which helps in improving the overall optical performance and reliability of the sensor.

The proposed sensor is capable of detecting different analytes ranging from RI 1.38 to 1.42, as shown in Table 1. An analyte is a specific substance or chemical component in a sample which is being identified, measured, or detected by a sensor or any analytical device. In the context of SPR biosensors, the analyte typically refers to the bio-chemical targets such as proteins, cells, or small molecules that interact with the sensor surface, causing a measurable change in the optical response.

1. Design Methodology and Simulation

In COMSOL Multiphysics 6.2, a two-dimensional (2D) geometry was employed to model the cross-sectional profile of the photonic crystal fiber, and the 'Electromagnetic Waves, Frequency Domain (emw)' physics interface, available under the Wave Optics module, was utilized to perform mode analysis. The flowchart, as shown in Figure 1, illustrates the main steps followed in this research. It gives a clear overview of the process, including the design, simulation, and analysis stages, thus providing a structured overview of the entire design and simulation process carried out in this work. Each block in the flowchart corresponds to a specific stage that is explained in detail in the subsequent sections. Starting from the geometrical modeling of the V-shaped PCF structure, followed by assigning material with the boundary conditions and designing the meshing structure of the core, thereafter simulation methodology, and finally, analyzing the confinement loss by optimizing the parameters has been shown in the flow diagram.

1.1 Geometrical Modeling

To maintain structural simplicity, the designed geometry incorporates only two distinct types of air holes extending along the fiber length, with diameters defined as $d1 = 0.3\,p$ (smaller holes) and $d2 = 0.65\,p$, where $p = 0.8\,\mu m$ represents the pitch, i.e., the center-to-center spacing between adjacent air holes can be observed in Figure 2. A smaller pitch typically enhances coupling between the core and the plasmonic layer, which is crucial for strong SPR excitation; thus, the pitch was optimized accordingly (Abdelghaffar et al., 2023; Zhang et al., 2017).

In proximity to the plasmonic metal layer, both air holes were scaled down to diameter d1 to enhance optical coupling between the guided mode and the metal interface. Abdelghaffar et al. (2023) emphasized that optimizing air-hole diameter helps achieve high sensitivity while maintaining single-mode operation. The plasmonic metal layer was positioned in a semicircular configuration of diameter d1, centered at a height $h = 1.2p$, with a thickness of $tg = 40\,\mu m$, oriented downward toward the fiber core; a gold layer thickness around 40–50 nm often yields strong resonance with acceptable loss, while thicknesses beyond this can dampen the evanescent field, reducing sensitivity (Johnson & Christy, 1972).

1.2 Material Assignment

The assigning of the material to the proposed model is depicted in Figure 3. In the process of material

Category	Examples of Analytes	Approximate Refractive Index (RI) Range	Application Area
Biological Fluids	Blood plasma, Serum, Cerebrospinal fluid, Tear fluid, Urine (concentrated)	1.38 – 1.40	Medical diagnostics, fluid analysis
Proteins/Biomolecules	Albumin, Immunoglobulin G (IgG), Antibodies, High-concentration glucose solutions	1.39 – 1.41	
Cells and Bacteria	Red blood cells, Bacterial membranes (e.g. E. coli)	1.40 – 1.41	Infection monitoring, cell analysis
Chemical Solutions	Glycerol–water mixtures, Sucrose–water mixtures	1.38 – 1.41	Chemical sensing, industrial monitoring
Cancer Cells (Majeed & Ahmad, 2024)	Malignant cell structures (e.g. MCF-7 and A549), basal cells	1.39 – 1.42	Cancer detection (early-stage diagnosis)

Table 1. Potential Category of Different Bio-chemical Analytes in RI range of 1.38 to1.42

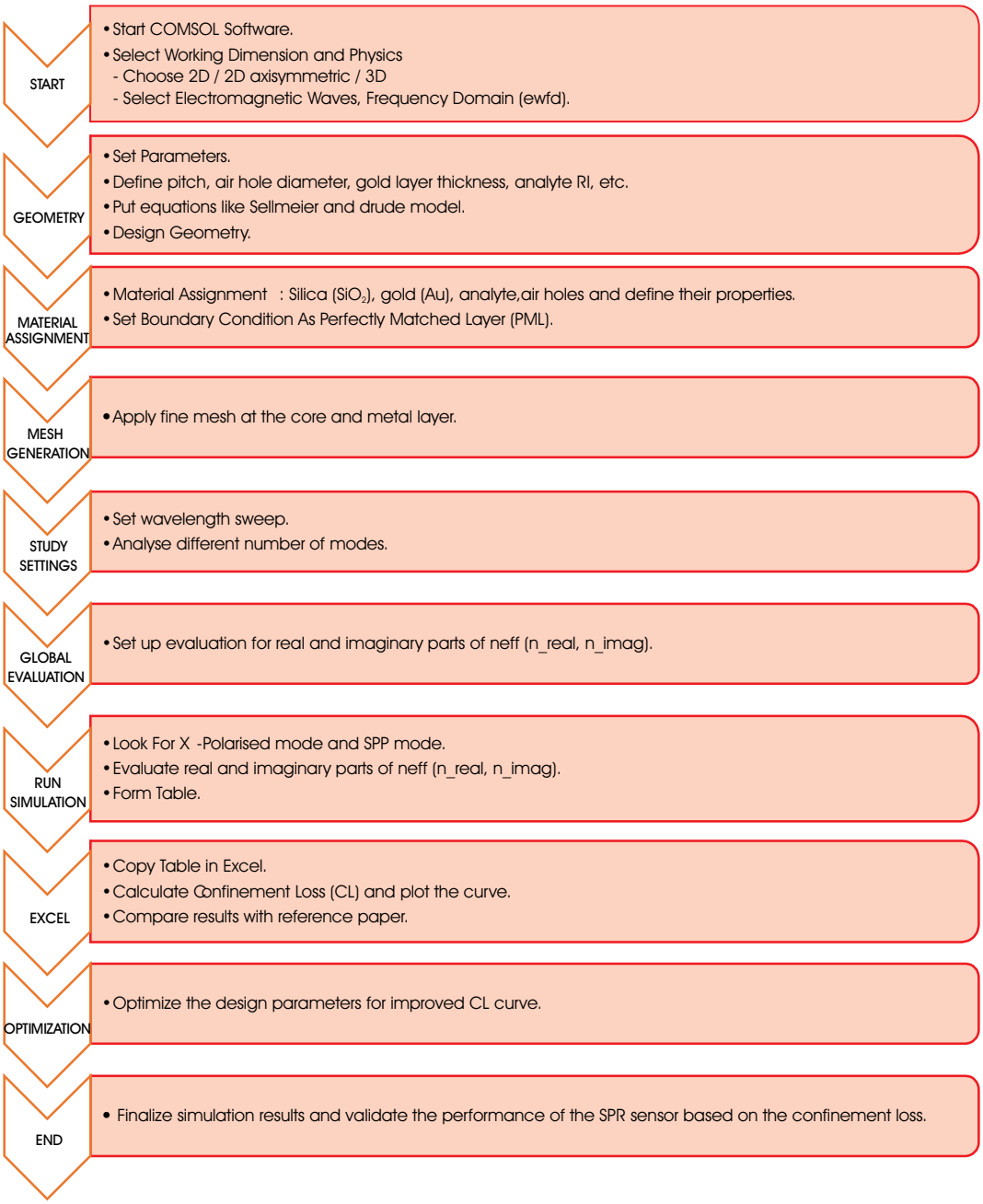

Figure 1. Process Flow-Diagram for Design Analysis of V Shaped SPR Sensor

assignment, air holes were assigned at first in grey color, which helps in confinement of the light. After this, the background material of the core was set as fused silica, shown in light blue color, which formed the main body of the fiber. The green color depicts the V-shaped analyte region near the core that interacts with guided light used for sensing. A thin gold layer displayed in yellow color was applied to enable surface plasmon resonance. In the last process of assignment, the perfectly matched layer is assigned as the outermost layer, which is shown in dark blue color in Figure 3. This layer is added to absorb outgoing waves and avoid reflection during simulation. All the materials were assumed to be non-magnetic and lossless, except for the metal, whose complex permittivity accounts for absorption losses.

Fused silica was selected as the background material.

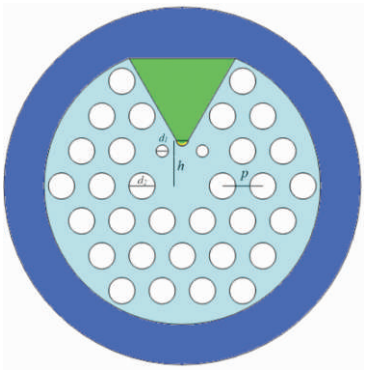

Figure 2. Geometrical Model Showing Various Structural Dimensions Along the Fiber Length

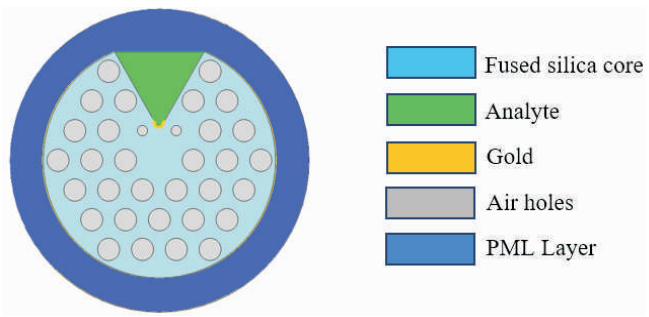

Figure 3. Assigning of Materials in Proposed Model

Its wavelength-dependent refractive index was modeled using the Sellmeier equation, given by Equation 1.

$$n^2(\lambda) = 1 + \frac{B_1\lambda^2}{\lambda^2 - C_1} + \frac{B_2\lambda^2}{\lambda^2 - C_2} + \frac{B_3\lambda^2}{\lambda^2 - C_3} \quad (1)$$

Where B_1, B_2, B_3, C_1, C_2 and C_3 are Sellmeier coefficients whose values are considered as B_1= 0.69616300, B_2= 0.407972600, B_3= 0.897479400 and the values for C_1, C_2 and C_3 are defined as C_1= 4.67914826 x 10^{-3} μm^2, C_2= 1.3512063 x 10^{-3} μm^2 and C_3= 97.9340025 μm^2. Similarly, in Equation 1, λ represents the wavelength expressed in µm and n represents the wavelength-dependent refractive index of the fused silica core (Lide, 2003). The complex permittivity of gold was defined using the Drude model to account for its frequency-dependent plasmonic behavior, which is shown in Equation 2.

$$\varepsilon_{Au}(\omega) = \varepsilon_\infty - \frac{\omega_D^2}{\omega(\omega + j\gamma_D)} - \frac{\nabla\in \Omega_L^2}{(\omega^2 - \Omega_L^2) + j\mathbb{\Gamma}_L\omega} \quad (2)$$

Here in equation (2), $\nabla\in = 1.09$ is the weighting factor, ε_∞ = 5.9673 is the permittivity at high frequency, ω is the angular frequency, $\omega^2 / 2\pi$ = 2113.6 THz is the plasma frequency, the damping frequency $\gamma_D / 2\pi$ is 15.92 THz and the frequency of the Lorentz oscillator $\Omega_L / 2\pi$ is 650.07 THz and the spectral width $\mathbb{\Gamma}_L / 2\pi$ is 104.86 THz (Johnson & Christy, 1972). To avoid unwanted reflections from the edges of the simulation area and to mimic an open space, Perfectly Matched Layers (PMLs) were added around the outer boundaries of the model (Berenger, 1994).

1.3 Meshing

Meshing discretizes the computational domain into a finite number of smaller sub-regions (called elements), which allows the numerical solution of partial differential equations using the finite element method (FEM). The quality and density of the mesh significantly influence the accuracy and convergence of the simulation results. Figure 4 shows a meshed model of the proposed sensor. To ensure high simulation accuracy and precise evaluation of confinement loss, the "Finer" mesh setting was selected.

1.4 Simulation and Study

In this section, various optical modes were analyzed, and the proposed sensor model was simulated to evaluate its electromagnetic response and confinement characteristics. This simulation considers only x-polarized light, which refers to light whose electric field oscillates along the x-axis. Also, this polarization in this direction

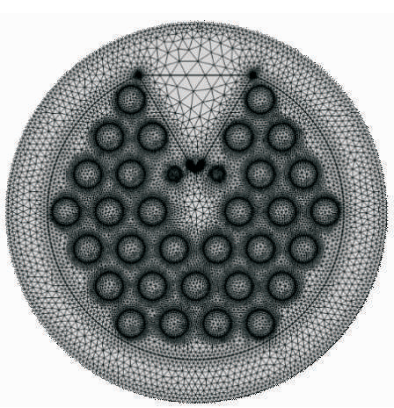

Figure 4. Proposed Meshed Model using the Finite Element Method (FEM)

facilitates the maximum energy transfer from the core mode to the surface plasmon polariton (SPP) mode (Maier, 2007). The surface wave in SPP mode travels along the metal–dielectric interface due to the interaction between light and free electrons. At a specific resonance wavelength, the x-polarized guided mode strongly couples with the SPP mode, resulting in near-complete energy transfer from the core to the metal surface. This leads to a sharp confinement loss peak, which is the key for detecting changes in the surrounding refractive index. Figures 5(a, b) show the x-polarized mode and SPP mode having a refractive index (RI) of 1.42 at 1180 nm. The optical response of the proposed sensor was studied over a wavelength range of 600 nm to 1200 nm.

Changing the air hole diameter affects the light confinement and coupling efficiency in the PCF. Larger diameters improve confinement but may reduce plasmonic interaction, while smaller diameters increase loss. Thus, air hole diameters were optimized accordingly, as it was crucial for balancing sensitivity and confinement

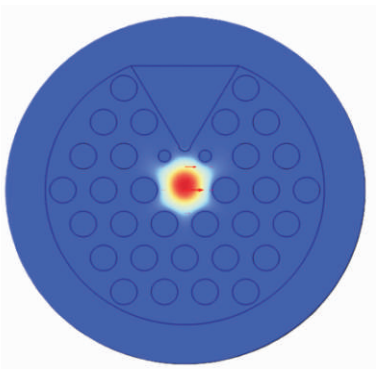

(a)

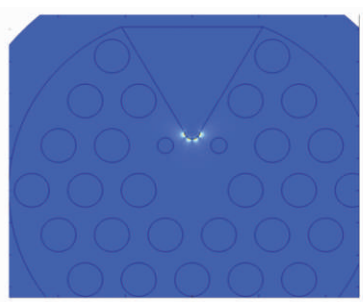

(b)

Figure 5. (a) X-polarsied Mode at 1180 nm, (b) SPP mode at 1180 nm with 1.42 RI

loss (Rifat et al., 2015). The gold layer thickness is crucial for SPR sensor performance; an optimal thickness enhances plasmonic coupling, while too thick or too thin layers can reduce sensitivity and increase losses (Das & Sen, 2024).

3. Results and Discussion

Figure 6 illustrates the confinement loss (CL) spectrum, which is calculated using Equation 3 as described below:

$$\alpha\left(\frac{dB}{cm}\right) = 8.686 \times k_O Im(n_{eff}) \times 10^4 \quad (3)$$

In this equation, $k_o = 2\pi/\lambda$, which is a free-space wave number, λ is the operating wavelength in μm, and $Im(n_{eff})$is the imaginary part of the core effective RI (Szpulak et al., 2006). The Confinement Loss (CL) spectrum was analyzed to identify resonant wavelengths. The resonant wavelength is defined as the wavelength at which the peak of the confinement loss occurs, indicating maximum energy coupling between the guided and plasmonic modes. A clear shift in the resonance wavelength is evident as the RI increases, confirming the sensor's ability to detect subtle changes in the surrounding medium. Table 2 summarizes the resonant wavelengths and peak confinement loss observed for varying refractive index (RI) values ranging from 1.38 to 1.42.

3.1 Comparative Analysis

To evaluate the performance of the proposed SPR sensor, a comparison is conducted against other relevant studies in terms of refractive index (RI) range, peak confinement

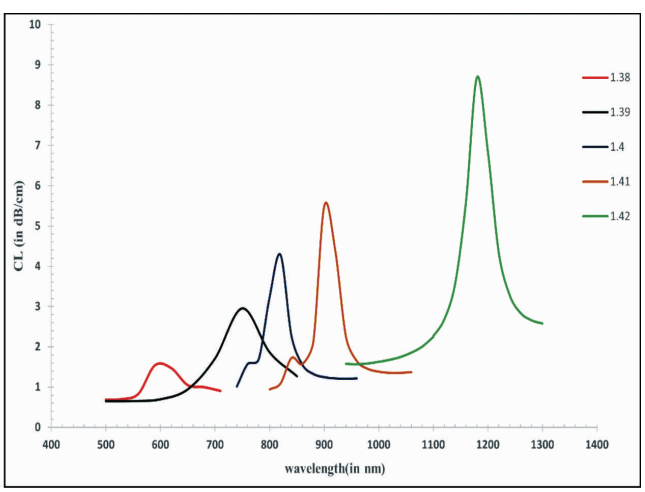

Figure 6. Confinement Loss Spectra for RI 1.38 to 1.42

Refractive Index	Resonant Wavelength (nm)	Peak Confinement Loss (dB/cm)
1.38	590	1.54
1.39	750	2.95
1.40	820	4.28
1.41	900	5.49
1.42	1180	8.69

Table 2. Resonant Wavelengths Corresponding to their Respective Refractive Index

loss (CL), and plasmonic material used. As shown in Table 3, Zhang et al. (2017) utilized a silver-graphene hybrid coating, achieving moderate CL (2–7 dB/cm) over the RI range 1.38–1.42, though the design involved complex fabrication and stability concerns due to silver oxidation. Ullah et al. (2024) achieved a peak CL of 12.36 dB/cm using a birefringent PCF structure with silver, indicating high sensitivity at RI = 1.41, but at the cost of higher signal loss. Zhang et al. (2018) employed a D-shaped PCF with gold, reaching up to 9 dB/cm CL in a narrow high-RI range (1.41–1.42), though with more complex geometry. There is always a trade-off between confinement loss (CL) and stability in SPR sensor design. While higher CL often enhances sensitivity by improving plasmonic coupling, it can also lead to greater signal attenuation and instability in detection performance. Conversely, lower CL improves stability and reduces losses but may compromise sensitivity. In contrast, the proposed work demonstrates a competitive CL range of 1.54–8.69 dB/cm using gold (Au) within a broad biosensing RI range of 1.38–1.42. The V-shaped PCF structure offers simpler fabrication, reliable biocompatibility, and stable performance, making it suitable for practical biosensing applications while maintaining low confinement loss.

Conclusion

In this paper, by optimizing the structural parameters and refining the geometrical design, an improved confinement loss curve is successfully achieved, as shown in Figure 3, indicating stronger plasmonic coupling and sharper resonance peaks. This enhancement directly translates to higher sensitivity in detecting variations in analyte refractive indices. The distinct and measurable shifts in resonance wavelengths corresponding to different analytes confirm the sensor's capability for accurate detection and differentiation.

Future Scope

Due to computational and scope constraints, the current analysis focused on X-polarized light, which is typically more sensitive in SPR sensing. Y-polarized light and multi-polarization conditions can be potential extensions of this work to explore its anisotropic behavior. This may reveal additional insights into polarization-dependent sensitivity and broaden the scope of practical applications. Furthermore, while gold (Au) has been utilized for its stability and plasmonic efficiency, alternative materials such as silver (Ag), aluminum (Al), and advanced multilayer coatings such as TiO_2 -Au or graphene-based composites can be considered as future work of this present research. These alternatives may offer improved plasmonic performance, greater sensitivity, and enhanced stability, thus opening new possibilities for optimization and application-specific tuning of the sensor design.

References

[1]. Abdelghaffar, M., Gamal, Y., El-Khoribi, R. A., Soliman, W., Badr, Y., Hameed, M. F. O., & Obayya, S. S. A. (2023). Highly sensitive V-shaped SPR PCF biosensor for cancer detection. *Optical and Quantum Electronics,* 55(5), 472.

https://doi.org/10.1007/s11082-023-04740-w

Study	Year	RI Range	CL Peak (dB/cm)	Plasmonic Material	Remark °
Zhang et al. (2017)	2017	1.38 – 1.42	~2 – 7	Silver-Graphene hybrid	Hybrid coating; enhanced tunability; oxidation prone; complex fabrication
Islam et al. (2020)	2020	1.33 – 1.41	Up to 12.36	Silver (Ag)	Birefringent PCF; CL peaks at RI=1.41
Ullah et al. (2024)	2024	1.41 – 1.42	Up to 9	Gold (Au)	D-shaped PCF; similar plasmonic material; complex geometry
Proposed work	2025	1.38 – 1.42	1.54 – 8.69	Gold (Au)	V-shaped PCF; simple geometry; optimized for biosensing; biocompatible material

° is based on structural design.

Table 3. Comparison of Confinement Loss (CL) in PCF-SPR Sensors

[2]. Berenger, J. P. (1994). A perfectly matched layer for the absorption of electromagnetic waves. *Journal of Computational Physics,* 114(2), 185-200.

https://doi.org/10.1006/jcph.1994.1159

[3]. COMSOL. (2023). *COMSOL Multiphysics Reference Manual.* Retrieved from

https://doc.comsol.com/6.1/doc/com.comsol.help.comsol/COMSOL_ReferenceManual.pdf

[4]. Das, S., & Sen, R. (2024). Design and numerical analysis of a pcf-spr sensor for early-stage malaria detection. *Plasmonics,* 19(5), 2565-2580.

https://doi.org/10.1007/s11468-024-02193-9

[5]. Gupta, B. D., & Sharma, A. K. (2005). Sensitivity evaluation of a multi-layered surface plasmon resonance-based fiber optic sensor: A theoretical study. *Sensors and Actuators B: Chemical,* 107(1), 40-46.

https://doi.org/10.1016/j.snb.2004.08.030

[6]. Gupta, B. D., & Verma, R. K. (2009). Surface plasmon resonance-based fiber optic sensors: principle, probe designs, and some applications. *Journal of Sensors,* 2009(1), 979761.

https://doi.org/10.1155/2009/979761

[7]. Hassani, A., & Skorobogatiy, M. (2006). Design of the microstructured optical fiber-based surface plasmon resonance sensors with enhanced microfluidics. *Optics Express,* 14(24), 11616-11621.

https://doi.org/10.1364/OE.14.011616

[8]. Homola, J. (2008). Surface plasmon resonance sensors for detection of chemical and biological species. *Chemical Reviews,* 108(2), 462-493.

https://doi.org/10.1021/cr068107d

[9]. Huraiya, M. A., Razzak, S. A., Tabata, H., & Ramaraj, S. G. (2024). New approach for a highly sensitive V-Shaped SPR biosensor for a wide range of analyte RI detection. *The Journal of Physical Chemistry C,* 128(36), 15117-15123.

https://doi.org/10.1021/acs.jpcc.4c04425

[10]. Islam, M. R., Jamil, M. A., Zaman, M. S. U., Ahsan, S. A. H., Pulak, M. K., Mehjabin, F., & Islam, M. (2020). Design and analysis of birefringent SPR based PCF biosensor with ultra-high sensitivity and low loss. *Optik,* 221, 165311.

https://doi.org/10.1016/j.ijleo.2020.165311

[11]. Johnson, P. B., & Christy, R. W. (1972). Optical constants of the noble metals. *Physical Review B,* 6(12), 4370.

https://doi.org/10.1103/PhysRevB.6.4370

[12]. Kretschmann, E., & Raether, H. (1968). Radiative decay of non radiative surface plasmons excited by light. *Zeitschrift für Naturforschung* A, 23(12), 2135-2136.

https://doi.org/10.1515/zna-1968-1247

[13]. Lide, D. R. (2003). *Geophysics, Astronomy, and Acoustics; Speed of Sound in Various Media.* CRC Handbook of Chemistry and Physics.

[14]. Maier, S. A. (2007). *Plasmonics: Fundamentals and Applications.* Springer, New York.

[15]. Majeed, M. F., & Ahmad, A. K. (2024). Design and analysis of a dual-core PCF biosensor based on SPR for cancerous cells detection. *Optical and Quantum Electronics,* 56(6), 1030.

https://doi.org/10.1007/s11082-024-06566-6

[16]. Mim, M. A., Khatun, M. R., Hossain, M. M., & Rahman, W. (2025). Advanced PCF-SPR biosensor design and performance optimization using machine learning techniques. *Optik,* 172391.

https://doi.org/10.1016/j.ijleo.2025.172391

[17]. Otto, A. (1968). Excitation of nonradiative surface plasma waves in silver by the method of frustrated total reflection. *Zeitschrift für Physik A Hadrons and Nuclei,* 216(4), 398-410.

https://doi.org/10.1007/BF01391532

[18]. Peng, L., Shi, F., Zhou, G., Ge, S., Hou, Z., & Xia, C. (2015). A surface plasmon biosensor based on a D-shaped microstructured optical fiber with rectangular lattice. *IEEE Photonics Journal,* 7(5), 1-9.

https://doi.org/10.1109/JPHOT.2015.2488278

[19]. Piliarik, M., Homola, J., Manıková, Z., & Čtyroký, J. (2003). Surface plasmon resonance sensor based on a single-mode polarization-maintaining optical fiber. *Sensors and Actuators B: Chemical,* 90(1-3), 236-242.

https://doi.org/10.1016/S0925-4005(03)00034-0

[20]. Rifat, A. A., Mahdiraji, G. A., Chow, D. M., Shee, Y. G., Ahmed, R., & Adikan, F. R. M. (2015). Photonic crystal fiber-based surface plasmon resonance sensor with selective analyte channels and graphene-silver deposited core. *Sensors,* 15(5), 11499-11510.

https://doi.org/10.3390/s150511499

[21]. Russell, P. (2003). Photonic crystal fibers. *Science,* 299(5605), 358-362.

https://doi.org/10.1126/science.1079280

[22]. Sardar, M. R., & Faisal, M. (2024). Dual-core dual-polished PCF-SPR sensor for cancer cell detection. *IEEE Sensors Journal,* 24(7), 9843-9854.

https://doi.org/10.1109/JSEN.2024.3358173

[23]. Sharma, A. K., Jha, R., & Gupta, B. D. (2007). Fiber-optic sensors based on surface plasmon resonance: a comprehensive review. *IEEE Sensors Journal,* 7(8), 1118-1129.

https://doi.org/10.1109/JSEN.2007.897946

[24]. Szpulak, M., Urbanczyk, W., Serebryannikov, E., Zheltikov, A., Hochman, A., Leviatan, Y., & Panajotov, K. (2006). Comparison of different methods for rigorous modeling of photonic crystal fibers. *Optics Express,* 14(12), 5699-5714.

https://doi.org/10.1364/OE.14.005699

[25]. Ullah, S., Chen, H., Guo, P., Song, M., Zhang, S., Hu, L., & Li, S. (2024). A highly sensitive d-shaped PCF-SPR sensor for refractive index and temperature detection. *Sensors,* 24(17), 5582.

https://doi.org/10.3390/s24175582

[26]. Verma, R., Gupta, B. D., & Jha, R. (2011). Sensitivity enhancement of a surface plasmon resonance based biomolecules sensor using graphene and silicon layers. *Sensors and Actuators B: Chemical,* 160(1), 623-631.

https://doi.org/10.1016/j.snb.2011.08.039

[27]. Willets, K. A., & Van Duyne, R. P. (2007). Localized surface plasmon resonance spectroscopy and sensing. *Annual Review of Physical Chemistry,* 58(1), 267-297.

https://doi.org/10.1146/annurev.physchem.58.032806.104607

[28]. Zhan, Y., Li, Y., Wu, Z., Hu, S., Li, Z., Liu, X., & Chen, Z. (2018). Surface plasmon resonance-based microfiber sensor with enhanced sensitivity by gold nanowires. *Optical Materials Express,* 8(12), 3927-3940.

https://doi.org/10.1364/OME.8.003927

[29]. Zhang, C., Li, Z., Jiang, S. Z., Li, C. H., Xu, S. C., Yu, J., & Man, B. Y. (2017). U-bent fiber optic SPR sensor based on graphene/AgNPs. *Sensors and Actuators B: Chemical*, 251, 127-133.

https://doi.org/10.1016/j.snb.2017.05.045

ABOUT THE AUTHORS

Dr. Nivedita Kar has a Ph.D. in Electronics and Communication Engineering from the University of Allahabad, Allahabad (2024), and a Master's degree in Electronics and Communication Engineering from SHIATS, Allahabad (2013). Her research involves the challenges and solutions of Embedded systems, Renewable Energy, Solar Cells, and Computational Modeling for Advanced Sensor Design. She is currently working as an Assistant Professor in the Department of Electronics Engineering at the Institute of Engineering and Rural Technology, Allahabad, with an experience of more than 10 years.

Dr. Ankita Kar has a Master's degree in Electronics and Communication Engineering from SHIATS, Allahabad (2013), and a Ph.D. in Electronics and Communication Engineering from the University of Allahabad, Allahabad (2024). She is currently working as an Assistant Professor in the Department of Electronics Engineering at the Institute of Engineering and Rural Technology, Allahabad. She has her experience in electronics with an emphasis on Optical Devices and Sensor Design fields.

Mayank Singh is a final-year B.Tech. student of Electronics Engineering at the Institute of Engineering and Rural Technology, Allahabad. His academic interests include Photonic Sensors, Optoelectronics, and Computational Modelling for Advanced Sensor Design.

Deepak Yadav is a final-year undergraduate engineering student of Electronics Engineering at the Institute of Engineering and Rural Technology, Allahabad. His academic interests include Photonic Sensors and its computational Modelling Design.